IEEE Access
Multidisciplinary | Rapid Review | Open Access Journal

Received 2 March 2024, accepted 23 March 2024, date of publication 28 March 2024, date of current version 9 April 2024.

Digital Object Identifier 10.1109/ACCESS.2024.3382822

RESEARCH ARTICLE

A Novel Mid-Infrared Transverse Magnetic Mode Pass Periodic Waveguide Polarizer With Low Reflections

HUMAIRA ZAFAR AND M. F. PEREIRA
Department of Physics, Khalifa University, Abu Dhabi, United Arab Emirates
Corresponding author: M. F. Pereira (mauro.pereira@ku.ac.ae)

This work was supported by Khalifa University under Award CIRA-2021-108.

ABSTRACT We propose a transverse magnetic (TM) pass polarizer based on a periodic waveguide on a silicon-on-insulator platform. The design is implemented on a 500nm-thick silicon layer surrounded by SiO_2. The polarizer operates in the mid-infrared (MIR) wavelength range of 3.1 µm to 3.6 µm, a crucial band for chemical and biological sensing, as well as environmental monitoring. While there is extensive documentation on polarizers in the near-infrared (NIR), there is a significant scarcity of research reports on polarizers in the MIR. This proposed polarizer demonstrates outstanding performance, characterized by ultra-low loss for the transmitted TM mode, minimal reflections of the undesired transverse electric (TE) mode, and exceptionally high loss for the transmitted TE mode. The TM insertion loss remains below 0.5dB over a wavelength range of 3.2 µm to 3.6 µm, as the TM mode operates in the subwavelength and low-loss radiation regimes. The transmitted TE power is remarkably small, falling below −30dB over a 300nm wavelength range. This is attributed to the TE mode operating in the high-loss radiation regime and the band gap region of the dispersion diagram. Furthermore, the reflected power of the undesired TE mode is significantly reduced (below −20dB) by incorporating the periodic waveguide in a directional coupler setup. The footprint of the polarizer is compact, measuring just 30 µm × 7 µm.

INDEX TERMS Mid infrared silicon photonics, semiconductor optoelectronic devices, nanoscale engineering, subwavelength gratings.

I. INTRODUCTION

Photonic integrated circuits (PICs) leverage silicon-on-insulator (SOI) as a key technological platform [1], which has been pioneered for over thirty years as an optical waveguide platform in data centers. This approach overcomes the limitations of electronic integrated circuits that have reached their maximum integration capacity [2], [3], positioning it as the most promising technology for designing high-density integrated chips [4], [5]. Recently, the MIR spectral region, extending beyond optical communication wavelengths, has garnered global research attention for its promising applications in diverse fields such as chemical and biological sensing, environmental monitoring, gas-trace detection, quantum photonics, lidar, CBRN detection, thermophotovoltaics and water quality monitoring applications [6], [7], [8], [9], [10]. The availability of efficient MIR Quantum Cascade Lasers (QCLs) sources, further fuels the interest in this range [11], [12]. However, despite its wealth of potential applications, the on-chip mid-IR photonics platform required to access these opportunities is still in a relatively immature stage. The minimal absorption loss in silicon material persists into the mid-infrared region (approximately 2 µm to 7 µm) [13], [14], encompassing sensing wavelengths relevant to gases like CO, CO2, NO, NH3, CH4, and OCS, highlighting that the influence of silicon photonics extends beyond the NIR wavelength range. Among various platforms such as SOI, germanium-on-silicon and Ge-on-SOI [15], [16], aluminum nitride-on-insulator [17], sapphire-on-silicon (SOS) [18], Chalcogenide Waveguides [19], SOI

The associate editor coordinating the review of this manuscript and approving it for publication was Weiren Zhu.

© 2024 The Authors. This work is licensed under a Creative Commons Attribution-NonCommercial-NoDerivatives 4.0 License.
For more information, see https://creativecommons.org/licenses/by-nc-nd/4.0/

stands out as the most widely favored material due to its ease of fabrication, established maturity, and stability. Prior research has affirmed that SOI continues to be a viable option up to 3.8 µm, owing to the substantial optical mode confinement facilitated by the significant refractive index contrast between Si and SiO_2 [20], [21]. In large refractive index contrast silicon waveguides, TE and TM modes exhibit varying profiles, confinement factors, and indices. Consequently, silicon photonic devices are typically optimized for one polarization to prevent performance degradation caused by undesired polarization. The introduction of unwanted polarization can occur through optical fibers lacking polarization control. While fiber-to-chip grating couplers serve as effective polarizers, edge couplers based on inverse tapers allow polarization-independent coupling, permitting any polarization into the waveguide. Moreover, imperfect operation of on-chip components like polarization splitters and rotators also introduces undesired polarization. Therefore, to avoid these undesired polarization fractions, on-chip polarizers can effectively mitigate crosstalk by removing these components [3]. As stated earlier in this section, the silicon material is a promising candidate for sensing applications in the mid-infrared spectrum, spanning approximately from 2 µm to 7 µm. Given that the TM mode exhibits lesser confinement within the waveguide and greater interaction with the surrounding medium, it inherently offers heightened sensitivity. Therefore, the utilization of the pure TM mode, characterized by low insertion loss, high extinction ratio, and minimal reflection, is highly desirable.

Light polarization control plays an important role in photonics, from the THz to the Ultraviolet range [22], [23]. Photonic integrated circuits are developed and optimized for a single polarization, requiring rigorous selection of the TE and TM modes. The on-chip polarization selection using polarization splitters, rotators, and polarizers has been extensively investigated in telecommunication bands [24], [25], [26], [27], [28], [29], [30], [31], [32], [33]. However, previous studies lack reporting on polarization control devices in the MIR wavelength range. The works cited in references [34], [35], [36] represent initial reports on polarization splitters and rotators in the MIR range, implemented on the SOI platform. On the other hand, polarization rotators have been reported on various platforms, including Germanium on silicon [37], silicon on sapphire [38], silicon-on-calcium-fluoride [39], and on InGaAs-InP [40]. These devices cover wavelength ranges of 9 µm to 11 µm, 4.55 µm, 4.29 µm to 4.65 µm, and 6.15 µm, respectively. Moreover, a polarization splitter on a GaAs nanowires has been reported in [41] at the operating wavelength of 3.5 µm.

Additionally, although polarizers are extensively documented in the NIR, enabling the desired mode to propagate with low insertion loss (IL) and blocking undesired modes with a high extinction ratio (ER), there are very few reports on their research in the MIR. For example, in [50], [51], and [52], TM-pass and TE-pass polarizers were discussed on a silicon-on-sapphire and SOI platforms at a wavelength of 2 µm. However, all other studies focus on NIR bands, encompassing plasmonic, bent, and periodic waveguides. Ultra-compact plasmonic polarizers show high IL and require additional metallization steps [53], while polarizers with low IL and small footprints can be achieved through bent silicon waveguides [27], [29]. On the other hand, a sophisticated method involves manipulating the effective index of a waveguide through the utilization of grating structures (periodic structures). In previous studies, various on-chip polarization control methods employing grating structures have been investigated. The majority of these methods are designed for the NIR wavelength ranges [28], [42], [43], [44], [45], [46], [47], [48], [49], [54], with the exception of [50], which is based on periodic structures and operates at a wavelength of 2 µm. Many of these suggested periodic configurations encounter issues with Bragg reflections. In order to prevent interference with other photonic components and lasers, it is essential to mitigate undesired reflections, which is the focus of efforts in References [28], [46], [47] to minimize their occurrence. In [47], the authors use a multimode waveguide as a Bragg grating, reflecting and converting TE light into higher-order modes, removing them through a tapered transition, reducing reflection loss by about 12 dB. Moreover, the grating mentioned in reference [46] reflects TE-polarized light in S, C, and L-bands, and tapered gratings extend operational bandwidth by diffracting TE light in O-band. In [28], the periodicity of the grating structure is manipulated to minimize reflection, effectively placing the undesired TE mode in the high-loss radiation regime instead of the bandgap regime. It was optimized for the L band using a 220 nm-thick silicon layer, resulting in a reflection loss of 13 dB (in the present design, we aim to further reduce reflections by incorporating the periodic waveguide into a directional coupler arrangement). Moreover, The MIR grating-based polarizer at [50], designed with a coupler arrangement at 2 µm wavelength, exhibits minimal reflection loss for the undesired mode. The design includes additional layers of SiN and metal depositions to absorb the undesired mode, adding complexity to its fabrication.

In this study, we have designed a periodic waveguide TM-pass polarizer for mid-infrared wavelengths beyond 3 µm. To the best of our knowledge, there is currently no reported polarizer for wavelengths greater than 3 µm on SOI platform. The design is implemented on an SOI platform, without the use of additional metal layers, ensuring complete CMOS compatibility. This configuration effectively minimizes TE back reflections in a directional coupler setup. A detailed performance comparison of this grating-based polarizer with those implemented on the SOI platform is documented in Table. 1.

II. POLARIZER DESIGN, OPERATION, AND FABRICATION FEASIBILITY

Fig. 1(a) and Figs. 1(b, g) show the 3D view and top views of the proposed grating-based transverse magnetic mode polarizer, along with cross-sections and the critical

TABLE 1. Performance Comparison of the proposed grating-based polarizer with the literature, showing reflection loss, insertion loss (IL), extinction ratio (ER), wavelengths, and footprints.

Ref	ER (dB)	IL (dB)	Reflection loss	Footprint	wavelength
[42]	≥ 20	≤ 0.42	Bragg reflections	12.2 µm	L band
[43]	≥ 21	≤ 1	Bragg reflections	13.6 µm × 1.3 µm	E-, S-, C-, L-, U- and O-bands
[44]	≥ 20	≤ 0.32	Bragg reflections	5.2 µm	1465nm to 1620 nm
[45]	≥ 20.8	≤ 1.2	Bragg reflections	7.21 µm	1520nm to 1590 nm
[46]	≥ 20	≤ 0.4	Bragg reflections in (S, C, L bands) diffraction (O band)	21.942 µm	O-, S-, C-, and L- bands
[47]	≥ 30	0.08	12.6 dB	30 µm	1450nm to 1650 nm
[28]	≥ 30	≤ 1	13 dB	21 µm × 0.5 µm	1500nm to 1600 nm
[48]	20	0.5	Bragg reflections	9 µm	1520nm to 1580nm
[49]	30	1	Bragg reflections	4 µm	1520nm to 1570nm
[50]	≥ 17	≤ 0.83	20dB	5.2 µm (coupler section only)	1850nm to 2110nm
This work	≥ 30 dB	≤ 0.5 dB	≥ 20 dB	30 µm × 7 µm	3200nm to 3400nm

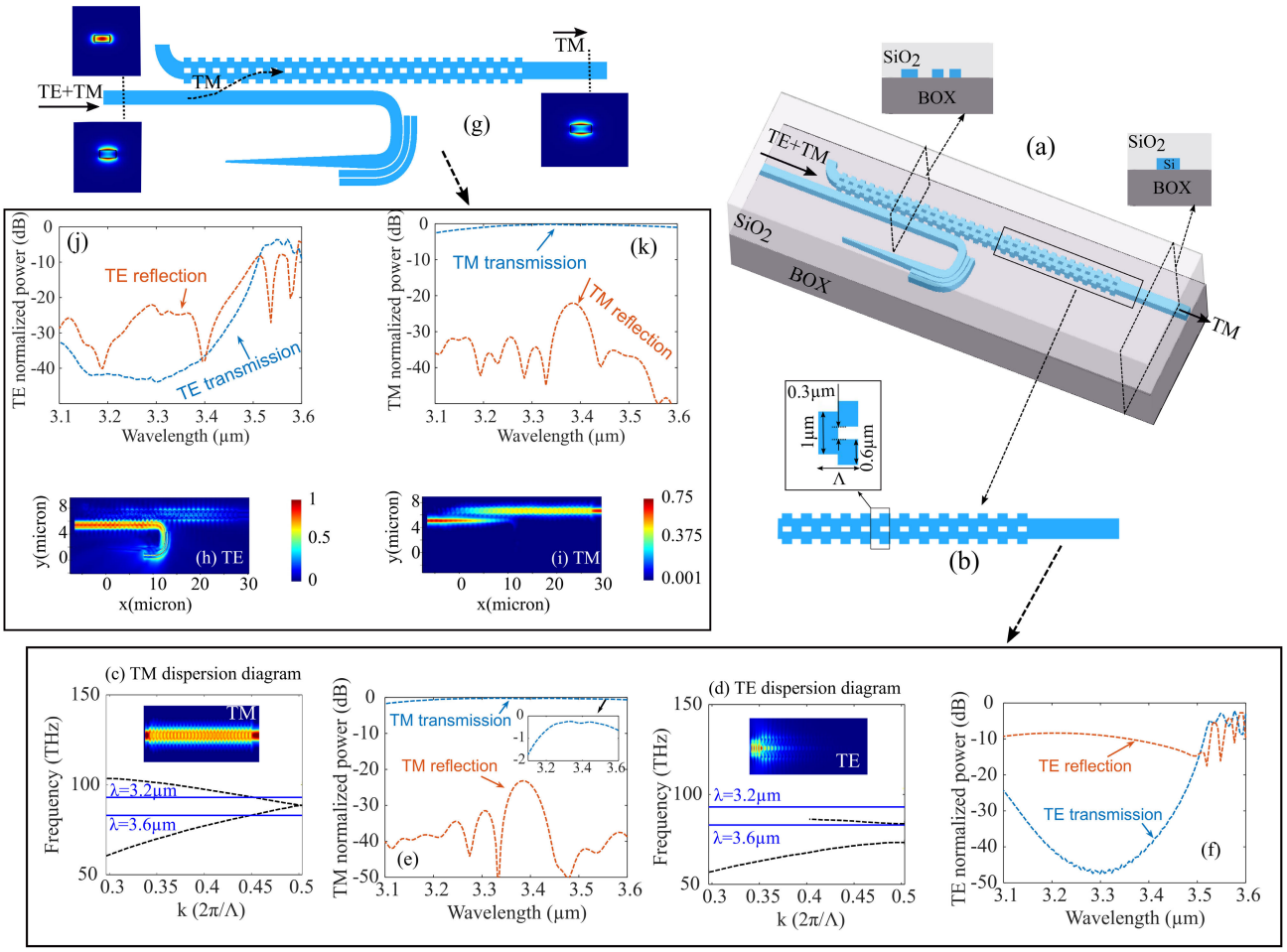

FIGURE 1. (a) Schematic illustration of the proposed TM-pass polarizer, (b) magnified view of the periodic waveguide, (c) dispersion relation illustrating TM mode in the periodic waveguide, with top view of TM light propagation in the inset at 3.2 µm wavelength, (d) dispersion relation for TE mode with top view of TE light propagation in the inset, (e) normalized transmitted and reflected TM powers, (f) normalized transmitted and reflected TE powers, where reflected powers are calculated at the input port, (g) top view of the proposed polarizer with mode profiles in the input and output cross sections, (h) top view illustrating TE mode propagation through the polarizer, demonstrating the absence of reflected light and no light reaching the output, (i) top view of TM mode propagation through the polarizer, allowing the light to propagate through. (j) normalized TE powers transmitted and reflected through the polarizer in the directional coupler arrangement, (k) normalized TM powers transmitted and reflected through the polarizer in the directional coupler arrangement.

parameters of the design. The main element of this design comprises a periodic waveguide. The waveguide exhibits a periodicity of $\Lambda = 1\,\mu m$ and a fill factor of 50%. The propagation of light within this periodic waveguide is intricately explained by the dispersion diagram, leading to various operational regimes [55], namely subwavelength,

Bragg reflection (photonic bandgap), and radiation. The functionality of the specified waveguide is meticulously optimized to facilitate the propagation of the desired mode without any loss, while concurrently ensuring that the undesired mode radiates outside the waveguide. This optimization is contingent upon factors such as the polarization state of the incident light, structural dimensions, and the free-space wavelength (λ). The proposed polarizer is defined on a 500 nm-thick silicon layer on a SOI platform, with a 2-micron buried oxide (BOX) and covered with SiO_2 from the top. One of the periodic waveguide unit cells is 1 µm wide, while the other unit cell is 1.5 µm wide, with a 300 nm slot in the center. These dimensions were optimized using the Lumerical 3D Finite-Difference Time-Domain (FDTD) computational method with refractive indices of 3.43 and 1.41 for Si and SiO_2, respectively, at a wavelength of 3.3 µm. The operating regime of the periodic waveguide (the magnified view of the waveguide is shown in Fig. 1(b)) can be determined from the dispersion diagrams plotted in Figures Fig. 1(c) and Fig. 1(d) for the TM and TE modes. The periodic waveguide dimensions are fine-tuned to minimize propagation loss for the TM mode while maximizing propagation loss for the TE mode. The dispersion diagrams exhibit horizontal blue lines corresponding to wavelengths of 3.2 µm and 3.6 µm. In terms of the TM mode (see Fig. 1(c) for TM dispersion diagram), the subwavelength condition ($\Lambda < \lambda/(2 \times n_{eff}$), where $n_{eff} = 1.62$) is met for the 3.6 µm wavelength, resulting in negligible TM mode loss due to the mode not perceiving the waveguide's periodicity at this wavelength. Conversely, at 3.2 µm wavelength, the subwavelength condition is not satisfied, causing the TM mode to enter a low-loss radiation regime. This observation is further observed by the TM transmission and reflection curves depicted in Fig. 1(e). The blue curve of TM transmission reveals insertion losses below 0.5 dB for wavelengths within the subwavelength regime. However, wavelengths in the low-loss transmission regime exhibit slightly higher insertion losses, approximately 0.8 dB at a wavelength of 3.2 µm, as depicted in the inset of Fig. 1(e). Additionally, the inset of Fig. 1(c) illustrates TM light propagation at 3.2 µm wavelength, clearly highlighting the occurrence of ultra-small radiations as anticipated from the dispersion diagram.

Additionally, the dispersion diagram for TE mode is illustrated in Fig. 1(d), revealing that the investigated wavelength range lies just above the first band gap. Fig. 1(d) highlights that the wavelength of 3.6 µm resides in the upper edge of the first band gap, suggesting the anticipation of Bragg reflections. Conversely, shorter wavelengths surpass the first band gap, resulting in the expectation of minimal reflections and high radiation loss. This observation is confirmed by Fig. 1(f), which illustrates low reflections at the shorter wavelengths, approximately −10dB. However, noticeable TE-reflected light is observed at the 3.5 µm to 3.6 µm wavelength range. Concurrently, the periodic waveguide effectively obstructs the undesired TE mode, as depicted by the blue curve in Fig. 1(f). This finding is further confirmed by the inset of Fig. 1(d), affirming the absence of TE light reaching the output.

The periodic waveguide effectively blocks the TE mode, resulting in negligible light reaching the output. However, approximately 10dB reflection loss is observed at the input port within the wavelength range of 3.1 µm to 3.4 µm, accompanied by strong reflections at wavelengths above 3.5 µm. Typically, minimizing back reflections from individual photonic components is crucial, as they may disrupt the operation and efficiency of other components, such as lasers. Utilizing this periodic waveguide in a directional coupler arrangement further reduces the occurrence of these reflections. In the directional coupler configuration, the input light is directed towards the conventional straight waveguide rather than the periodic waveguide (drop port). When utilizing the desired TM mode, the light efficiently couples with the periodic waveguide, resulting in a substantial power output from the periodic waveguide. Conversely, in the case of the undesired TE mode, a small fraction of the input TE power couples with the periodic waveguide, where it disperses without returning to the input waveguide. The remaining TE power disperses from the sharp bend of the input waveguide, further diminishing reflections at the input port (see Figs. 1(h) and (i). Fig. 1(g) illustrates the top view of the periodic waveguide, depicting mode profiles at the input and output of the polarizer. This coupler arrangement enables the TM mode to couple with the periodic waveguide from the input waveguide. The periodic waveguide allows the TM mode to propagate and reach the output. In contrast, the TE mode cannot couple with the periodic waveguide from the input waveguide due to phase mismatch. Only a small fraction of the coupled TE light is observed, which cannot reach the output due to the periodic waveguide blocking the TE mode. As a result, the extinction of the TE mode is enhanced in a coupled waveguide arrangement, remaining below −32 dB over a wavelength range of 300 nm. Furthermore, in this coupled waveguide arrangement, only the small amount of undesired TE-coupled light directed to the periodic waveguide is reflected back. A mixed TE and TM mode is launched at the input, but only the TM mode is achieved at the output. This is clearly observed in Fig. 1(h) and Fig. 1(i), showing the propagation of TE and TM modes through the polarizer, respectively. The TE mode is effectively blocked, resulting in negligible light at the output. Additionally, minimal reflected light is observed at the input, and most fraction of the undesired TE light radiates and scatters at the sharp 1 µm bend. The 1 µm bend is too sharp for the mode at these wavelengths, where two closely spaced waveguides have also been implemented to enhance the scattering and suppression of the undesired light. Fig. 1(j) further confirms these observations, clearly indicating that the TE reflected power is below -20dB in the wavelength range of 3.1 µm to 3.4 µm. However, wavelengths above 3.5 µm only show a slight improvement in the reduction of reflected TE light. This is due to the longer wavelengths in the input waveguide having a better mode overlap with

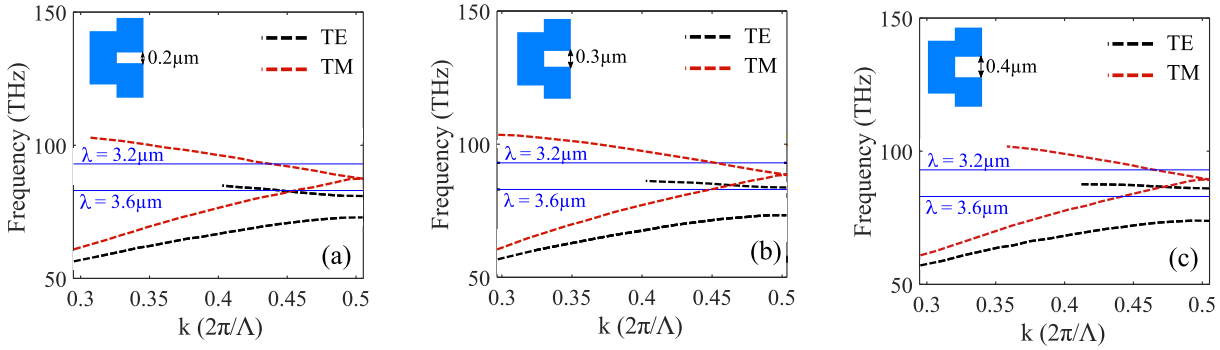

FIGURE 2. Dispersion relations illustrating TM and TE modes in the periodic waveguide with the slot widths of **(a)** 200 nm, **(b)** 300 nm, and **(c)** 400 nm.

the periodic waveguide, thereby increasing the likelihood of coupling to the periodic waveguide. As a result, this fraction of TE mode is observed at the input. To reduce these reflections at wavelengths above 3.5 µm, the width of the input waveguide must be increased, or the coupling gap should be widened. However, such adjustments will impact the performance for shorter wavelengths.

In the meantime, the input TM mode effectively couples to the periodic waveguide, with the maximum fraction of light observed at the output. This is clearly depicted in Fig. 1(e) and Fig. 1(k), which show TM transmitted and reflected powers in the single periodic waveguide and coupled waveguide arrangement, respectively. These figures indicate that there is no significant difference in the reflected and transmitted powers as expected. Hence, the suggested polarizer exhibits a broad performance range spanning 500 nanometers in wavelength. To expand this bandwidth further, it is necessary to optimize the structural parameters of the periodic waveguide to achieve the desired performance within the intended wavelength range.

The proposed design consists of a single-etch silicon waveguide on an SOI platform. Single-etch waveguides can be readily fabricated using optical lithography [29] and electron beam lithography [31]. A crucial factor influencing the performance of this polarizer is the slot width. We investigate the fabrication tolerance of the polarizer and its performance dependence on this critical parameter. The minimum feature size of the other parameters of this polarizer is highly flexible and can be achieved as designed using a standard and well-established CMOS fabrication facility. The influence of slot width on performance is examined using dispersion diagrams. Fig. 2 illustrates the calculated dispersion relations for slot widths of 200 nm, 300 nm, and 400 nm. The optimized results in Fig. 1 are obtained for a slot width of 300 nm. We also computed dispersion diagrams for slot widths of 200 nm and 400 nm. It is observed that as the slot width increases, longer wavelengths of the TE mode enter the stop band, while shorter wavelengths remain in the high-loss radiation regime. Conversely, reducing the slot width keeps all wavelengths in the radiation regime, resulting in weak reflections of the TE mode. Generally, there is a slight shift in the bands with changes in slot width, confirming that the TE mode remains highly lossy. Similarly, the TM mode stays in the subwavelength propagation regime and low-loss radiation regime for longer and shorter wavelengths, respectively. Overall, a change in slot width by ±100nm shows no impact on the performance of the polarizer, making it highly fabrication-friendly. The footprint of the polarizer is only 30 µm×7 µm, making it suitable for highly dense integrated circuits.

III. CONCLUSION

In summary, our proposed TM pass polarizer, implemented on a silicon-on-insulator platform with a periodic waveguide, excels in the critical mid-infrared wavelength range (3.1 µm to 3.6 µm). While there is abundant documentation regarding polarizers in the NIR, there is a notable lack of research reports addressing polarizers in the MIR spectrum. This polarizer showcases exceptional performance, ensuring ultra-low loss for the TM mode and minimizing reflections of the undesired TE mode. The mid-infrared spectral range, which goes beyond the wavelengths used in optical communication, has attracted worldwide research interest due to its promising applications in various fields like chemical and biological sensing, environmental monitoring, gas-trace detection, quantum photonics, and lidar applications. Despite the numerous potential applications, the on-chip mid-IR photonics platform needed to exploit these opportunities is still in a relatively early stage of development. The polarizer proposed for MIR in the provided wavelength range represents the first report of its kind.

REFERENCES

[1] M. R. Chaudhry, M. Zakwan, M. C. Onbasli, and A. Serpengüzel, "Symmetric meandering distributed feedback structures for silicon photonic circuits," *IEEE J. Sel. Topics Quantum Electron.*, vol. 26, no. 2, pp. 1–5, Mar. 2020.

[2] P. P. Absil, P. Verheyen, P. De Heyn, M. Pantouvaki, G. Lepage, J. De Coster, and J. Van Campenhout, "Silicon photonics integrated circuits: A manufacturing platform for high density, low power optical I/O's," *Opt. Exp.*, vol. 23, no. 7, pp. 9369–9378, 2015.

[3] D. Dai, J. Bauters, and J. E. Bowers, "Passive technologies for future large-scale photonic integrated circuits on silicon: Polarization handling, light non-reciprocity and loss reduction," *Light, Sci. Appl.*, vol. 1, no. 3, p. e1, Mar. 2012.

[4] H. Zafar, B. Paredes, I. Taha, J. E. Villegas, M. Rasras, and M. F. Pereira, "Compact and broadband adiabatically bent superlattice-waveguides with negligible insertion loss and ultra-low crosstalk," *IEEE J. Sel. Topics Quantum Electron.*, vol. 29, no. 6, pp. 1–9, Nov. 2023.

[5] H. Zafar, B. Paredes, J. Villegas, M. Rasras, and M. F. Pereira, "O-band TE-and TM-mode densely packed adiabatically bent waveguide arrays on the silicon-on-insulator platform," *Opt. Exp.*, vol. 31, no. 13, pp. 21389–21398, 2023.

[6] M. Clerici, D. Faccio, L. Caspani, M. Peccianti, O. Yaakobi, B. E. Schmidt, M. Shalaby, F. Vidal, F. Légaré, T. Ozaki, and R. Morandotti, "Spectrally resolved wave-mixing between near- and far-infrared pulses in gas," *New J. Phys.*, vol. 15, no. 12, Dec. 2013, Art. no. 125011, doi: 10.1088/1367-2630/15/12/125011.

[7] R. Soref, "Mid-infrared photonics in silicon and germanium," *Nature Photon.*, vol. 4, no. 8, pp. 495–497, Aug. 2010.

[8] M. F. Pereira and O. Shulika, *Terahertz Mid Infr. Radiation: Detection Explosives CBRN* (Using Terahertz). Dordrecht, The Netherlands: Springer, 2014.

[9] M. F. Pereira, "Microscopic approach for intersubband-based thermophotovoltaic structures in the terahertz and mid-infrared," *J. Opt. Soc. Amer. B*, vol. 28, no. 8, p. 2014, Aug. 2011.

[10] P. Cousin, A. Moumtzidou, A. Karakostas, L. Gounaridis, C. Kouloumentas, M. F. Pereira, A. Apostolakis, P. Gorrochategui, G. Aoust, and B. Lebental, *Improving Water Quality and Security With Advanced Sensors and Indirect Water Sensing Methods*. Cham, Switzerland: Springer, 2022, pp. 251–277

[11] M. Razeghi, N. Bandyopadhyay, Y. Bai, Q. Lu, and S. Slivken, "Recent advances in mid infrared (3–5μm) quantum cascade lasers," *Opt. Mater. Exp.*, vol. 3, no. 11, pp. 1872–1884, Nov. 2013.

[12] D. O. Winge, M. Franckié, C. Verdozzi, A. Wacker, and M. F. Pereira, "Simple electron-electron scattering in non-equilibrium Green's function simulations," *J. Phys. Conf. Ser.*, vol. 696, Mar. 2016, Art. no. 012013, doi: 10.1088/1742-6596/696/1/012013.

[13] G. Z. Mashanovich, M. M. Milošević, M. Nedeljkovic, N. Owens, B. Xiong, E. J. Teo, and Y. Hu, "Low loss silicon waveguides for the mid-infrared," *Opt. Exp.*, vol. 19, no. 8, p. 7112, 2011.

[14] S. A. Miller, M. Yu, X. Ji, A. G. Griffith, J. Cardenas, A. L. Gaeta, and M. Lipson, "Low-loss silicon platform for broadband mid-infrared photonics," *Optica*, vol. 4, no. 7, p. 707, 2017.

[15] D. Marris-Morini, V. Vakarin, J. M. Ramirez, Q. Liu, A. Ballabio, J. Frigerio, M. Montesinos, C. Alonso-Ramos, X. L. Roux, S. Serna, D. Benedikovic, D. Chrastina, L. Vivien, and G. Isella, "Germanium-based integrated photonics from near-to mid-infrared applications," *Nanophotonics*, vol. 7, no. 11, pp. 1781–1793, 2018.

[16] R. Morgan, C. Heidelberger, D. Kharas, K. Cahoy, and C. Sorace-Agaskar, "Low-loss germanium-on-silicon waveguides and ring resonators for the mid-wave infrared," in *CLEO: Science and Innovations*. Washington, DC, USA: Optica Publishing Group, 2022.

[17] P. T. Lin, H. Jung, L. C. Kimerling, A. Agarwal, and H. X. Tang, "Low-loss aluminium nitride thin film for mid-infrared microphotonics," *Laser Photon. Rev.*, vol. 8, no. 2, pp. L23–L28, Mar. 2014.

[18] R. Shankar, I. Bulu, and M. Lončar, "Integrated high-quality factor silicon-on-sapphire ring resonators for the mid-infrared," *Appl. Phys. Lett.*, vol. 102, no. 5, Feb. 2013, Art. no. 051108.

[19] B. J. Eggleton, B. Luther-Davies, and K. Richardson, "Chalcogenide photonics," *Nature Photon.*, vol. 5, no. 3, pp. 141–148, Mar. 2011.

[20] G. Z. Mashanovich, F. Y. Gardes, D. J. Thomson, Y. Hu, K. Li, M. Nedeljkovic, J. Soler Penades, A. Z. Khokhar, C. J. Mitchell, S. Stankovic, R. Topley, S. A. Reynolds, Y. Wang, B. Troia, V. M. N. Passaro, C. G. Littlejohns, T. Dominguez Bucio, P. R. Wilson, and G. T. Reed, "Silicon photonic waveguides and devices for near-and mid-IR applications," *IEEE J. Sel. Topics Quantum Electron.*, vol. 21, no. 4, pp. 407–418, Jul. 2015.

[21] M. Nedeljkovic, A. Z. Khokhar, Y. Hu, X. Chen, J. S. Penades, S. Stankovic, H. M. H. Chong, D. J. Thomson, F. Y. Gardes, G. T. Reed, and G. Z. Mashanovich, "Silicon photonic devices and platforms for the mid-infrared," *Opt. Mater. Exp.*, vol. 3, no. 9, p. 1205, 2013.

[22] A. Karabchevsky, A. Hazan, and A. Dubavik, "All-optical polarization-controlled nanosensor switch based on guide-wave surface plasmon resonance via molecular overtone excitations in the near-infrared," *Adv. Opt. Mater.*, vol. 8, no. 19, Oct. 2020, Art. no. 2000769.

[23] J. Wu, Y. Yang, Y. Qu, X. Xu, Y. Liang, S. T. Chu, B. E. Little, R. Morandotti, B. Jia, and D. J. Moss, "Graphene oxide waveguide and micro-ring resonator polarizers," *Laser Photon. Rev.*, vol. 13, no. 9, 2019, Art. no. 1900056.

[24] Y. Xu, Z. Tian, X. Meng, and Z. Chai, "Methods and applications of on-chip beam splitting: A review," *Frontiers Phys.*, vol. 10, Sep. 2022, Art. no. 985208.

[25] L. Sun, Y. Zhang, Y. He, H. Wang, and Y. Su, "Subwavelength structured silicon waveguides and photonic devices," *Nanophotonics*, vol. 9, no. 6, pp. 1321–1340, Jun. 2020.

[26] B. Troia, F. De Leonardis, M. Lanzafame, T. Muciaccia, G. Grasso, G. Giannoccaro, C. E. Campanella, and V. M. N. Passaro, "Design and optimization of polarization splitting and rotating devices in silicon-on-insulator technology," *Adv. OptoElectronics*, vol. 2014, pp. 1–16, Feb. 2014.

[27] H. Zafar, Y. Zhai, J. E. Villegas, F. Ravaux, K. L. Kennedy, M. F. Pereira, M. Rasras, A. Shamim, and D. H. Anjum, "Compact broadband (O, E, S, C, L & U bands) silicon TE-pass polarizer based on ridge waveguide adiabatic S-bends," *Opt. Exp.*, vol. 30, no. 6, pp. 10087–10095, 2022.

[28] H. Zafar, M. Odeh, A. Khilo, and M. S. Dahlem, "Low-loss broadband silicon TM-pass polarizer based on periodically structured waveguides," *IEEE Photon. Technol. Lett.*, vol. 32, no. 17, pp. 1029–1032, Sep. 1, 2020.

[29] H. Zafar, P. Moreira, A. M. Taha, B. Paredes, M. S. Dahlem, and A. Khilo, "Compact silicon TE-pass polarizer using adiabatically-bent fully-etched waveguides," *Opt. Exp.*, vol. 26, no. 24, p. 31850, 2018.

[30] H. Zafar, M. F. Pereira, K. L. Kennedy, and D. H. Anjum, "Fabrication-tolerant and CMOS-compatible polarization splitter and rotator based on a compact bent-tapered directional coupler," *AIP Adv.*, vol. 10, no. 12, Dec. 2020, Art. no. 125214.

[31] H. Zafar, R. Flores, R. Janeiro, A. Khilo, M. S. Dahlem, and J. Viegas, "High-extinction ratio polarization splitter based on an asymmetric directional coupler and on-chip polarizers on a silicon photonics platform," *Opt. Exp.*, vol. 28, no. 15, p. 22899, 2020.

[32] W. Shi, X. Wang, C. Lin, H. Yun, Y. Liu, T. Baehr-Jones, M. Hochberg, N. A. F. Jaeger, and L. Chrostowski, "Silicon photonic grating-assisted, contra-directional couplers," *Opt. Exp.*, vol. 21, no. 3, p. 3633, 2013.

[33] M. Nikufard and A. Rostami Khomami, "Hybrid plasmonic polarization splitter using three-waveguide directional coupler in InGaAsP/InP," *Opt. Quantum Electron.*, vol. 48, no. 5, pp. 1–7, May 2016.

[34] J. Wang, C. Lee, B. Niu, H. Huang, Y. Li, M. Li, X. Chen, Z. Sheng, A. Wu, W. Li, X. Wang, S. Zou, F. Gan, and M. Qi, "A silicon-on-insulator polarization diversity scheme in the mid-infrared," *Opt. Exp.*, vol. 23, no. 11, p. 15029, 2015.

[35] T. Hu, M. S. Rouifed, H. Qiu, X. Guo, C. G. Littlejohns, C. Liu, and H. Wang, "A polarization splitter and rotator based on a partially etched grating-assisted coupler," *IEEE Photon. Technol. Lett.*, vol. 28, no. 8, pp. 911–914, Apr. 15, 2016.

[36] T. Hu, H. Qiu, Z. Zhang, X. Guo, C. Liu, M. S. Rouifed, C. G. Littlejohns, G. T. Reed, and H. Wang, "A compact ultrabroadband polarization beam splitter utilizing a hybrid plasmonic Y-branch," *IEEE Photon. J.*, vol. 8, no. 4, pp. 1–9, Aug. 2016.

[37] K. Gallacher, R. W. Millar, U. Griškevičū, M. Sinclair, M. Sorel, L. Baldassarre, M. Ortolani, R. Soref, and D. J. Paul, "Ultra-broadband mid-infrared Ge-on-Si waveguide polarization rotator," *APL Photon.*, vol. 5, no. 2, Feb. 2020, Art. no. 026102.

[38] A. Rostamian, J. Guo, S. Chakravarty, H. Yan, C.-J. Chung, E. Heidari, and R. T. Chen, "Grating-coupled silicon-on-sapphire polarization rotator operating at mid-infrared wavelengths," *IEEE Photon. Technol. Lett.*, vol. 31, no. 5, pp. 401–404, Mar. 1, 2019.

[39] B. Kumari, R. K. Varshney, and B. P. Pal, "Design of a promising silicon slot waveguide-based ultra-short low loss efficient polarization rotator for the mid-IR," *Optik*, vol. 180, pp. 71–83, Feb. 2019.

[40] C.-J. Chung, J. Midkiff, K. M. Yoo, A. Rostamian, J. Guo, R. T. Chen, and S. Chakravarty, "InP-based polarization rotator-splitter for mid-infrared photonic integration circuits," *AIP Adv.*, vol. 9, no. 1, Jan. 2019, Art. no. 015303.

[41] F. Wang, Y. Chen, C. Li, T. Ma, X. Wang, K. Yu, and L. Li, "Ultracompact and broadband mid-infrared polarization beam splitter based on an asymmetric directional coupler consisting of GaAs–CaF_2 hybrid plasmonic waveguide and GaAs nanowire," *Opt. Commun.*, vol. 502, Jan. 2022, Art. no. 127418.

[42] Y. Dong, Y. Liu, Y. Xu, and B. Zhang, "An ultra-broadband design of TM-Pass/TE-Stop polarizer based on multistage Bragg gratings," *Photonics*, vol. 9, no. 6, p. 409, Jun. 2022.
[43] S. Wu, Z. Guo, T. Feng, J. Xiao, and X. S. Yao, "Compact and ultra-broadband all-silicon TM-pass and TE-reflected polarizer using grating based weakly coupled nanowires," *Opt. Exp.*, vol. 30, no. 17, p. 29844, 2022.
[44] Z. Xu, T. Lyu, and X. Sun, "Interleaved subwavelength gratings strip waveguide based TM pass polarizer on SOI platform," *IEEE Photon. J.*, vol. 12, no. 2, pp. 1–10, Apr. 2020.
[45] Y. He, Y. Zhang, R. Zhang, L. Sun, and Y. Su, "Ultra-compact and broadband silicon polarizer employing a nanohole array structure," *Opt. Lett.*, vol. 46, no. 2, p. 194, 2021.
[46] J. Zhang, L. Xu, D. Mao, Y. D'Mello, W. Li, S. Lessard, and D. V. Plant, "All-silicon multi-band TM-pass polarizer on a 220 nm SOI enabled by multiplexing grating regimes," *Opt. Exp.*, vol. 30, no. 1, p. 326, 2022.
[47] S. Wu, J. Hao, Z. Zhao, and X. S. Yao, "Low loss and high extinction ratio all-silicon TM-pass polarizer with reflection removal enabled by contra-mode conversion Bragg-gratings," *Opt. Exp.*, vol. 29, no. 17, pp. 27640–27652, 2021.
[48] X. Guan, P. Chen, S. Chen, P. Xu, Y. Shi, and D. Dai, "Low-loss ultra-compact transverse-magnetic-pass polarizer with a silicon subwavelength grating waveguide," *Opt. Lett.*, vol. 39, no. 15, pp. 4514–4517, 2014.
[49] D. W. Kim, M. H. Lee, Y. Kim, and K. H. Kim, "Ultracompact transverse magnetic mode-pass filter based on one-dimensional photonic crystals with subwavelength structures," *Opt. Exp.*, vol. 24, no. 19, p. 21560, 2016.
[50] Z. Guo and J. Xiao, "Ultracompact silicon-based TE-pass power divider for 1.55/2 μm dual-wavelength," *Opt. Eng.*, vol. 59, no. 9, 2020, Art. no. 097103.
[51] A. E.-S. Abd-Elkader, E. ELDamarawy, M. F. O. Hameed, and S. S. A. Obayya, "Ultra-compact SOS-based bi-metallic TM-pass polarizer," *Opt. Quantum Electron.*, vol. 54, no. 4, p. 257, Apr. 2022.
[52] Z. Guo and J. Xiao, "Ultracompact TE 0-and TE 1-pass/TM 0-and TM 1-stop dual-mode polarizer for 1.55/2 μm dual-wavelength using silicon-based cross-like hybrid plasmonic waveguides," *JOSA B*, vol. 37, no. 12, pp. 3604–3613, 2020.
[53] X. Sun, M. Z. Alam, S. J. Wagner, J. S. Aitchison, and M. Mojahedi, "Experimental demonstration of a hybrid plasmonic transverse electric pass polarizer for a silicon-on-insulator platform," *Opt. Lett.*, vol. 37, no. 23, p. 4814, 2012.
[54] M. Barona-Ruiz, C. Pérez-Armenta, A. Ortega-Moñux, G. Wangüemert-Pérez, Ì. Molina-Fernández, P. Cheben, and R. Halir, "Broadband and low-loss TM-pass polarizer using tilted subwavelength structures," *Opt. Exp.*, vol. 30, no. 21, p. 38930, 2022.
[55] R. Halir, P. J. Bock, P. Cheben, A. Ortega-Moñux, C. Alonso-Ramos, J. H. Schmid, J. Lapointe, D.-X. Xu, J. G. Wangüemert-Pérez, Í. Molina-Fernández, and S. Janz , "Waveguide sub-wavelength structures: A review of principles and applications," *Laser Photon. Rev.*, vol. 9, no. 1, pp. 25–49, Jan. 2015.

HUMAIRA ZAFAR received the Ph.D. degree from the Masdar Institute, Khalifa University (KU), Abu Dhabi, in collaboration with Massachusetts Institute of Technology (MIT). She is a Postdoctoral Fellow with KU. Her research with KU focuses on the development of novel photonic components for 6G networks and medical applications. She is also involved in the development of high-speed, high-density, and low-power optical interconnects to replace traditional electrical interconnects. She has experience in the design, nanofabrication, and characterization of silicon photonic and optoelectronic devices. She is also involved in material characterization using SEM/EDX, TEM/EELS, FIB, and Lamella preparation. She has contributed to several tapeouts with IME Singapore and GlobalFoundries, New York.

M. F. PEREIRA received the Ph.D. degree from the Optical Sciences Center, The University of Arizona. He was a Research Associate with CBPF, The University of Rostock, and TU-Berlin; a Visiting Lecturer with the University of Bremen; a Senior Researcher with the Tyndall Institute; a Professor and the Chair of Theory of Semiconductor Materials and Optics, Sheffield Hallam University; and the Head of the Department of Condensed Matter Theory, Institute of Physics of the Academy of Sciences of Czech Republic, before joining Khalifa University as a Professor and the Chair of the Physics Department. His research is focused on non-equilibrium greens functions (NEGF) many body theory of transport and optics of semiconductor materials, combining fundamental mathematical physics with applications to device development, with a current emphasis on the protection of water critical infrastructures and metabolomics. In 2011, he was named as a SPIE Fellow for his contributions to the theory of semiconductor materials and optics. He received the SPIE Innovation Awards in Quantum Sensing and Nano Electronics and Photonics, in 2019, for contributions to science and his service through organizing NATO TERA-MIR and COST. He created the TERA-MIR concept unifying THz and mid infrared radiation. He was the Chair of COST ACTION MP1204: TERA-MIR Radiation: Materials, Generation, Detection and Applications; and the Series of NATO TERA-MIR Conferences, in 2009, 2012, 2015, and 2018. He coordinates the TERA-MIR Network (http://www.tera-mir.org).